Indian Journal of Chemistry
Vol. 62, October 2023, pp. 1030-1039
DOI: 10.56042/ijc.v62i10.6180

Computational spectroscopic investigation of the effect of nitrosyl bonding type on molecular properties in iron tetracarbonyl nitrosyl complex

Özge Öztarakçı & Duran Karakaş*

Cumhuriyet University, Science Faculty, Chemistry Department, 50140, Sivas, Turkey

E-mail: dkarakas@cumhuriyet.edu.tr

Received 27 September 2022; accepted (revised) 5 September 2023

eq-$[Fe(CO)_4(NO)]^+$ ($\mathbf{C_{2v}}$), ax-$[Fe(CO)_4(NO)]^+$ ($\mathbf{C_{3v}}$),eq-$[Fe(CO)_4(NO)]^-$ ($\mathbf{C_s}$) and ax-$[Fe(CO)_4(NO)]^-$ ($\mathbf{C_s}$) complex ions have been designed for iron tetracarbonyl nitrosyl. Experimental C–O stretching frequencies of the complex with C_{2v} symmetry have been used to determine the optimal computation level. The optimal level for the complexes has been determined as BVP86/LANL2DZ/6-31G(d). Optimized structures of complex ions with C_{2v}, C_{3v} and C_s point groups have been found at the optimal computational level in the gas phase. During the optimization process, it is seen that the eq-$[Fe(CO)_4(NO)]^-$ complex with C_s symmetry is transformed into the ax-$[Fe(CO)_4(NO)]^-$ complex with the C_s symmetry. From the bond angles, IR spectra and ^{13}C NMR spectra, it is predicted that the iron atom in each of the complexes is a triangular bipyramidal ligand field. From the C-O stretching frequencies in the carbonyl stretching region and the Fe-C bond force constants, it has been estimated that complex with C_{2v} point group can be used as CO-releasing material (CORM). Optical conductivity (ΔE), hardness (η), Mulliken electronegativity (χ) and electrophilicity index (ω) values of the complexes have been calculated from the highest occupied molecular orbital energy (E_{HOMO}) and lowest energy unoccupied molecular orbital energy (E_{LUMO}) values. The calculated values show that the optical conductivity, softness, nucleophilicity index and basicity strength of the complex with C_s point group are higher than those of the other complexes.

Keywords: Metal carbonyls, Metal nitrosyls, Spectroscopic properties, CORM, Optical conductivity, Computational studies

Iron, one of the most abundant elements on our planet, forms numerous and diverse complexes. Iron carbonyls are one of them. Carbonyl forms complexes with almost all transition metals. Metal carbonyls consisting of only CO and metal are called homoleptic, while metal carbonyls containing ligands other than carbonyl are called heteroleptic metal carbonyls.

The oxidation state of iron in homoleptic or heteroleptic metal carbonyls can be -2, -1, 0, +1, +2, +3, +4 and +6. The most common of these oxidation steps are -2, -1, 0 and +2 [1-5]. Due to the strong π-acceptor property of carbonyl, high oxidation states are not uncommon in iron carbonyl complexes. Complexes of iron in -1 and +1 oxidation states form dimers to obey the 18-electron rule[6].

Like other metal carbonyls, iron carbonyls have important functions in many types of catalysis. Catalytic reactions involving iron carbonyls are of great variety, such as C-C bond formation, hydrogenation, and amination[6-11]. Hydrogenases that catalyze reversible hydrogen evolution and oxidation at fast rates (about 104 s^{-1} (Ref. 12)) without any overpotential under physiological conditions have been found to have iron carbonyl at their active metal site[13-15].

Research interest in iron carbonyls has been further increased by their use in therapeutic applications[16]. CO ligands in iron carbonyls can decompose under appropriate external stimuli such as photolysis, redox and ligand exchange. This property makes iron carbonyls another important application. It is known that decomposed CO from metal carbonyls has various physiological functions such as anti-inflammatory, protection of tissues from reperfusion damage in operations, vasodilation, anti-apoptotic, anti-proliferative, anti-hypoxia[17-24]. Therefore, iron carbonyls serve as potential sources of CO for medical applications, and CO releasing materials (CORMs) are areas of intense pursuit. Such physiological functions of CO are surprising. Because CO is a toxic molecule that is gaseous under normal conditions. The lethal dose for an adult human is about 1950 ppm[25]. The CO molecule binds to hemoglobin (Hb) approximately 200 times stronger than oxygen to form carboxyhemoglobin (COHb). In fact, it is an endogenous messenger molecule in the human body[26,27].

A wide variety of model systems have been developed in recent years, especially regarding the importance of iron nitrosyl intermediates in biochemistry and medicine[28-34]. The long-known flexible bonding motifs and bonding patterns of NO ligand are still debated and re-explored today[35]. The NO ligand can be linearly or angularly attached to the central metal atom. It is considered NO or NO^+ when bonded linearly, and NO or NO^- when bonded angularly. It is assumed that each type of bonding gives a different number of electrons to the metal. Mainly iron carbonyl nitrosyl complexes are obtained by reduction of Fe(II) initiators and they are usually stabilized by bulky and strong π-donor ligands such as $[C\{Si(CH_3)_3\}_3]$ (Ref. 36), cyclic (alkyl)-(amino)carbenes[37] or N-heterocyclic carbenes (NHCs)[38]. In such a way, iron tetracarbonyl nitrosyl complex ion with C_{2v} symmetry was synthesized by J. Bohnenberger and I. Krossing and some computational studies were carried out on the complex ion[36].

In this study, we considered that the NO ligand is linearly bonded to the central iron atom in the NO^+ form and angularly bonded in the NO^- form. We designed the schematic structures in Fig. 1 for $[Fe(CO)_4(NO)]^{+/-}$ complex ions. We aimed to investigate the molecular structures, spectroscopic properties, CORMs and optical conductivity of these complex ions using computational methods.

Methods and Techniques

Schematic structure of eq-$[Fe(CO)_4(NO)]^+$ (C_{2v}), ax-$[Fe(CO)_4(NO)]^+$ (C_{3v}), eq-$[Fe(CO)_4(NO)]^-$ (C_s) and ax-$[Fe(CO)_4(NO)]^-$ (C_s) complexes were drawn in Gauss View 6.0.16 program[39]. Benchmark analysis was performed according to the experimental C-O stretching frequencies of the complex with C_{2v} symmetry. The BVP86/LANL2DZ/6-31G(d) level was determined as the most optimal calculation level. Quantum chemical calculations were performed in the gas phase in the Gaussian 16 Revision C.01 program at the optimal calculation level[40]. The BVP86 method, also referred to as BP86, is a hybrid density functional theory (DFT) method. This method includes Becke88 exchange corrections[41] and Perdew86 correlation corrections[42]. It fits with remarkable accuracy the exact Hartree-Fock exchange energies for a wide variety of atomic and molecular systems and provides better performance than functionals with two or more parameters. LANL2DZ/6-31G(d) is a mixed basis set. The LANL2DZ basis set was used to model the iron atomic orbitals. This basis set is a frequently used basis set for the elements beyond the third order in the periodic table, using the effective nuclear potential for electrons close to the nucleus[43]. The 6-31G(d) polarized basis set was used to model the orbitals of C, N and O atoms in complex ions. This basis set, which adds d functions to heavy atoms, is widely used in modeling medium-sized systems[44]. ^{13}C NMR spectra and chemical shift values of the complexes at the BVP86/LANL2DZ/6-31G(d) level were calculated using the GIAO method. TMS was used as reference. The highest occupied molecular orbital energy (E_{HOMO}) and the lowest unoccupied molecular orbital energy (E_{LUMO}) were obtained from the molecular orbital energy diagrams of the complex ions. optical conductivity (ΔE), hardness (η), Mulliken electronegativity (χ) and electrophilicity index (ω) values of the complexes were calculated from equation (1-4)[45].

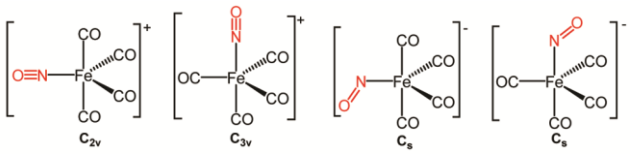

Fig. 1 — Schematic structures of the studied complex ions

$$\Delta E = E_{LUMO} - E_{HOMO} \quad \text{... (1)}$$

$$\eta = \frac{E_{LUMO} - E_{HOMO}}{2} \quad \text{... (2)}$$

$$\chi = \frac{-E_{HOMO} - E_{LUMO}}{2} \quad \text{... (3)}$$

$$\omega = \frac{\chi^2}{2\eta} \quad \text{... (4)}$$

Findings and Discussion

Benchmark analysis

In computational chemistry, the process of determining the optimal calculation level for an atomic or molecular system is called benchmark analysis. An experimentally measured property of the system is calculated at various levels in order to perform benchmark analysis. The level that gives the best agreement between the calculated and measured values is chosen as the optimal calculation level. For the eq-$[Fe(CO)_4(NO)]^+$ (C_{2v}) complex ion considered in this study, the C-O stretching frequencies were measured experimentally. Therefore, the CO

stretching frequencies of the conformer with C_{2v} symmetry were calculated at the levels of HF/LANL2DZ (1), HF/LANL2DZ/6-31G(d) (2), HF/DEF2TZVPP (3), B3LYP/LANL2DZ (4), B3LYP/LANL2DZ/6-31G (d) (5) B3LYP/DEF2TZVPP (6), BVP86/LANL2DZ (7), BVP86/LANL2DZ/6-31G(d) (8) and BVP86/DEF2TZVPP (9). The calculated harmonic C-O stretching frequencies are given in Table 1 together with the experimental frequencies.

The average of the differences between the calculated and experimental frequencies can be taken as a benchmark. Therefore, the average of differences was calculated from eq. (5) and given in the last column of Table 1.

$$AD = \frac{|C - E|}{N} \quad \ldots (5)$$

Here, AD is the average of differences, C is the calculated value, E is the experimental value, and N is the number of values. The level with the lowest average of differences can be taken as the optimal calculation level. As can be seen from Table 1, for the complex with C_{2v} symmetry, the level with the lowest average of differences is level 8. This calculation level is BVP86/LANL2DZ/6-31G(d). C-O stretching frequencies calculated at the BVP86/LANL2DZ/6-31G(d) level are more consistent with the experimental frequencies than the frequencies calculated at the BP86/def2TZVPP-D3B level given in the literature[36].

Ground state molecular structures

Molecular properties depend on molecular structures. Therefore, the determination of molecular structures has an important role in predicting molecular properties. Spectroscopic methods such as X-ray diffraction, IR, NMR, UV-VIS are widely used to experimentally determine molecular structures. In order to determine the molecular structures computationally, the designed molecular structure is optimized with optimal quantum chemical method and IR, NMR and UV-VIS spectra of the molecule can be calculated. If the molecule is properly designed and optimized by a suitable quantum chemical computational method, the optimized structures and the ORTEP diagrams obtained from the X-ray diffraction method almost overlap. The molecular structure parameters of the molecules can be found from the optimized structures obtained computationally.

The ground state molecular structures of the $[Fe(CO)_4(NO)]^{+/-}$ complex ions designed in this study were optimized in the gas phase at the BVP86/LANL2DZ/6-31G(d) level and their optimized structures with atomic labeling are given in Fig. 2.

As seen in Fig. 2, two different conformers of the $[Fe(CO)_4(NO)]^+$ complex ion with C_{2v} and C_{3v} symmetry have been optimized. The Gibbs free energies of the conformers with C_{2v} and C_{3v} symmetry calculated at 298.15 K and 1.00 atm are -706.6562 H and -706.6403 H, respectively. The conformer with C_{2v} symmetry has only 0.4327 eV lower energy than the conformer with C_{3v} symmetry. This low energy difference means that both conformers can form.

As given in Fig. 1, two conformers with C_s symmetry were designed for the $[Fe(CO)_4(NO)]^-$ complex ion, in which the NO^- ion is in both equatorial and axial positions. When these conformers were optimized, only the structure with C_s symmetry in Fig. 2 was found in which NO^- was in the axial position. In other words, as a result of the optimization, the eq-$[Fe(CO)_4NO]^-$ conformer was transformed into the ax-$[Fe(CO)_4NO]^-$ conformer. The Gibbs free energy for the ax-$[Fe(CO)_4NO]^-$ conformer is -706.9903 H. This result shows that

Table 1 — Calculated harmonic C-O stretching frequencies (cm^{-1}) for the eq-$[Fe(CO)_4(NO)]^+$ complex with C_{2v} symmetry, experimental frequencies and average of differences (AD)

Level	A_1	A_2	B_1	B_2	AD
1	2420	2415	2409	2408	266.2
2	2557	2553	2549	2547	405.7
3	2545	2540	2536	2535	393.2
4	2138	2100	2094	2079	43.0
5	2263	2228	2224	2210	85.5
6	2259	2219	2215	2199	77.2
7	2052	2000	1997	1980	138.5
8	2170	2122	2120	2105	16.5
9	2166	2113	2112	2094	24.5
Exp.	2183	2144	2137	2119	–

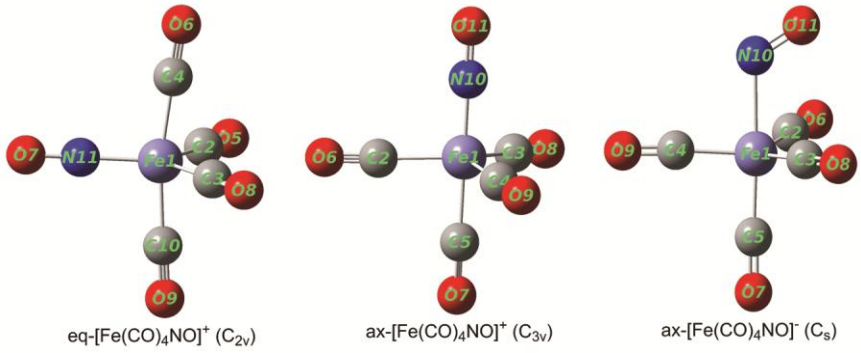

Fig. 2 — Ground state molecular structures of $[Fe(CO)_4(NO)]^{+/-}$ complex ions obtained at the BVP86/LANL2DZ/6-31G(d) level

when NO^- ion is bonded to the equatorial position, Gibbs free energy of the conformer is quite high and the most stable structure will be formed when the NO^- ion is bonded to the axial position. Some molecular structure parameters of the conformers with C_{2v}, C_{3v} and C_s symmetry of $[Fe(CO)_4(NO)]^{+/-}$ complex ions are given in Table 2.

As seen in Table 2, equatorial Fe-C bonds are shorter than axial Fe-C bonds for all three complexes. This can be explained by the hybridization type of the iron atom in the complexes. In all of the complex ions, the central iron atom hybridized to dsp^3. Not all hybrid orbitals formed in this hybridization are identical. According to the Bent rule, dp hybrids form the axial Fe-C bonds and sp^2 hybrids form the equatorial Fe-C bonds[46]. Since the s-character of sp^2 hybrids is higher than the s-character of dp hybrids and the s orbitals are closer to the nucleus, equatorial Fe-C bonds are expected to be shorter than axial Fe-C bonds. Findings from the calculations confirm this prediction. In addition, the lengths of the experimental Fe-C bonds are given as 1.838 Å in the literature without making any axial-equatorial distinction[36]. Fe-N and N-O bonds in complex with Cs symmetry are longer than those of complexes with C_{2v} and C_{3v} symmetry, and Fe-C bonds are shorter. The longer Fe-N bond in the complex with C_s symmetry indicates that the NO^- ligand is weaker π-acceptor than the CO ligand. The strongest π-acceptor ligand in the spectrochemical series is CO. The CO ligand is isoelectronic with NO^+. Significant back bonding also occurs in NO^+ complexes. The longer N-O bond in the complex with C_s symmetry than that of the complexes with C_{2v} and C_{3v} symmetry is related to the degree of N-O bond. The degree of N-O bond is about three in the NO^+ ligand and about two in the NO^- ligand. The lower N-O bond degree in the NO^- ligand causes the N-O bond to be longer. As seen in Table 2, the C-O bonds in the complex with C_s symmetry are longer than those of the complexes with C_{2v} and C_{3v} symmetry. This result shows that the Fe-C bonds are strengthened in the C_s symmetrical complex, while the C-O bonds are weakened by back-bonding. Therefore, the CORM property of the C_s complex should be lower than that of the C_{2v} and C_{3v} complexes. In addition, the negative charge of the $[Fe(CO)_4(NO)]^-$ complex indicates that the carbonyl ligand will more easily gain electrons for back

Table 2 — Some molecular structure parameters of the complexes with C_{2v}, C_{3v} and C_s symmetry

	C_{2v}	C_{3v}	C_s
Bond	Length (Å)	Length (Å)	Length (Å)
Fe-$C_{(eq)}$	1.838	1.837	1.767
Fe-$C_{(ax)}$	1.843	1.840	1.776
Fe-N	1.696	1.690	2.099
N-O	1.152	1.150	1.207
C-$O_{(eq)}$	1.150	1.150	1.181
C-$O_{(ax)}$	1.148	1.149	1.180
Angle	Degree (°)	Degree (°)	Degree (°)
$C_{(eq)}$-Fe-$C_{(eq)}$	113.3	119.3	121.5
$C_{(eq)}$-Fe-$C_{(ax)}$	87.3	85.2	91.9
$C_{(eq)}$-Fe-$N_{(eq)}$	123.3	–	–
$C_{(eq)}$-Fe-$N_{(ax)}$	–	94.8	85.5
$C_{(ax)}$-Fe-$C_{(ax)}$	170.1	–	–
$C_{(ax)}$-Fe-$N_{(ax)}$	–	180.0	177.7
Fe-N-O	180.0	179.9	120.5
Fe-$C_{(ax)}$-O	179.5	180.0	178.3
Fe-$C_{(eq)}$-O	178.4	178.3	178.8

bonding from the central iron atom and will strengthen the Fe-C bond. The strengthening of the Fe-C bond reduces the CORM feature.

As seen in Table 2, the angles between the ligands in the equatorial positions are approximately 120°, the angles between the ligands in the axial positions are approximately 180°, and the angles between the ligands in the axial-equatorial positions are approximately 90°. These findings indicate that the central iron atom is a triangular bipyramidal ligand field.

In addition, while the Fe-N-O angle is about 180° in complexes with C_{2v} and C_{3v} symmetry, it is about 120° in complexes with Cs symmetry. This result shows that the NO^+ ligand binds to the central atom linearly and NO^- is angularly bound. This can be explained by the steric numbers of donor nitrogen atoms in NO^+ and NO^- ions. The steric number of the donor nitrogen atom in the NO^+ ion is two and it has sp hybridized. One of the sp hybrid orbitals forms the N-O σ-bond with the oxygen atom, while the other sp hybrid orbital contains the lone pair. NO^+ ligand forms the Fe-N σ-bond by donating the lone pair in the sp hybrid orbital to the central iron atom. Since there are no other lone pairs on nitrogen atom, the Fe-N-O bond angle is linear. Whereas, in the NO^- ion, the steric number of the donor nitrogen atom is three and the nitrogen atom hybridization type is sp^2. The lone pair in one of the sp^2 hybrid orbitals is donated to the central iron atom to form a Fe-N σ-bond. The lone pair in the other sp^2 hybrid orbital causes the Fe-N-O bond angle to be angular due to lone pair-bond pair repulsion.

IR spectra in the carbonyl stretching region and symmetry labeling of the peaks

Since the C-O bond stretching frequencies in metal carbonyls are observed in a region that is quite different from the other bond stretching frequencies in the molecule (2200-1850 cm^{-1}), the molecular structure can be determined by considering only the C-O bond stretching modes. Therefore, this method is called the carbonyl factored force field method. There are studies on the applications of this method in the literature[47,48].

Applications of the carbonyl factored force field method predict C-O stretching peaks of symmetry types $2A_1+B_1+B_2$ for the complex with C_{2v}, $2A_1+E$ for the complex with C_{3v}, and $3A'+A''$ for the complex with C_s symmetry. Since all vibrations of these symmetry species are IR active, four C-O stretching peaks should be observed for the complex with C_{2v} symmetry, three for the complex with C_{3v} (two C-O stretching peaks occur at the same frequency since the E symmetry species is binary degenerate), and four for the complex with C_s symmetry.

In this study, IR spectra of the complexes with C_{2v}, C_{3v} and C_s symmetry in the C-O stretching region were calculated at the BVP86/LANL2DZ/6-31G(d) level. According to the calculated IR spectra, the N-O stretching frequencies also fall into the C-O stretching region. The calculated IR spectra for the complexes and the symmetry labeling of the peaks are given in Fig. 3.

Examining Fig. 3, the number of C-O stretching peaks predicted by the carbonyl factored force fields method is seen for each of the complexes. The C-O stretching frequencies of the complex with Cs symmetry, which have A′ and A″ symmetries, are quite close to each other. Therefore, C-O stretching peaks with A′ and A″ symmetries appear as a single

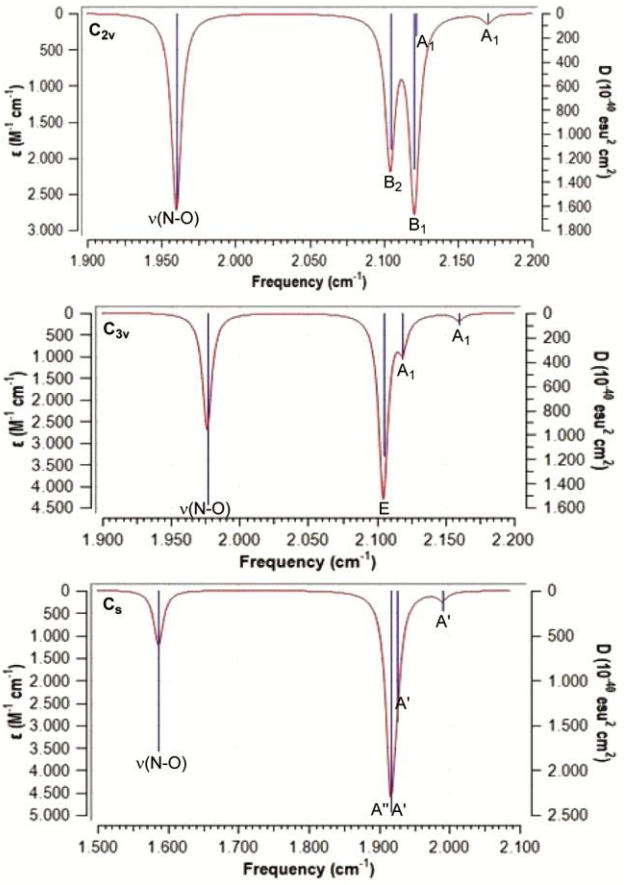

Fig. 3 — IR spectra of the complexes with C_{2v}, C_{3v} and C_s symmetry calculated at the BVP86/LANL2DZ/6-31G(d) level and symmetry labeling of peaks

peak. The frequencies of the peaks, whose symmetry labeling is given in Fig. 3, are given in Table 3.

As seen in Table 3, the C-O stretching frequencies of the complex with C_{2v} symmetry are greater than those of the complexes with C_{3v} and C_s symmetry. The high C–O stretching frequency can be explained by the fundamental equation (eq. 6) of IR spectroscopy[49].

$$\bar{\nu} = \frac{1}{2\pi c}\sqrt{\frac{k}{\mu}} \quad \text{... (6)}$$

In the equation (6), In the relation, k represents the force constant, μ the reduced mass of the bonded atoms, and $\bar{\nu}$ the vibrational frequency. The reduced mass for C-O has the same value in all complexes and the other parameters in the equation are constant. The bond stretching vibration frequency is then directly proportional to the square root of the bond force constant. In general, bond force constants are also directly proportional to bond dissociation energies. The higher the bond force constant, the higher the vibration frequency. According to this evaluation, the order of $k(C_s)<k(C_{3v})<k(C_{2v})$ can be made among the C-O bond stretching force constants of the complexes. A large C-O bond force constant indicates weak carbonyl back-bonding and a low Fe-C bond force constant. The decrease in the Fe-C bond force constant indicates that iron carbonyls can be used as CO-releasing materials (CORMs) in therapeutic applications. According to this evaluation, the order of using the investigated complexes as CORMs can be made as $C_s<C_{3v}<C_{2v}$. This result indicates that the ax-$[Fe(CO)_4(NO)]^-$ complex with Cs symmetry cannot be used as (CORM). Angular binding and negative charge of NO^- ligand in this complex caused strong back-bonding, strengthening of Fe-C bonds and inhibition of CO emission by taking electrons from the central iron atom of the CO ligand to the π^* molecular orbital. These findings obtained by vibration spectroscopy are also compatible with the bond lengths obtained from the optimized structures.

^{13}C NMR spectra and chemical shift values

Nuclear magnetic resonance (NMR) spectroscopy is a widely used technique for molecular structure determination. Equivalent and enantiotopic atoms in the molecule and their chemical shift values can be determined by NMR spectroscopy. Atoms that replace each other by rotation around an axis of symmetry are called equivalent atoms, and atoms that replace each other only by reflection are called enantiotopic atoms. Equivalent or enantiotopic atoms peak at the same chemical shift value in the NMR spectrum[49].

In this study, the ^{13}C NMR spectra and chemical shift values of the complexes were calculated at the BVP86/LANL2DZ/6-31G(d) level using the Gauge-Independent Atomic Orbital (GIAO) method. TMS was used as reference. TMS was first optimized in the gas phase at the BVP86/6-31G(d). Then, the shielding of carbon atoms in TMS was calculated as 188.22 ppm with the GIAO method at the same level. Chemical shift values of carbon atoms in complex ions were calculated from eq (7).

$$\delta = \Sigma_{TMS} - \Sigma \quad \text{... (7)}$$

Here, δ is the chemical shift value of carbon atoms according to TMS, Σ_{TMS} is the shielding of carbon atoms in TMS, and Σ is the shielding of carbon atoms in the complexes. The ^{13}C NMR spectra of the complexes with C_{2v}, C_{3v} and C_s symmetry were calculated at the GIAO-BVP86/LANL2DZ/6-31G(d) level and the spectra are given in Fig. 4.

As seen in Fig. 4, there are two peaks with the same degeneracy in the ^{13}C NMR spectrum of the complex with C_{2v} symmetry. Among these peaks, the low ppm value belongs to the 2C and 3C carbons in the equatorial position, and the high ppm value belongs to the 4C and 10C carbons in the axial position (Fig. 2). This result shows that 2C-3C and 4C-10C are equivalent. As seen in Fig. 2, when the molecule with C_{2v} symmetry is rotated 180° around a C_2-axis passing through the Fe1-N11-O7 bond axis,

Table 3 — Frequencies (cm^{-1}) of calculated C-O and N-O stretching peaks of complex ions with C_{2v}, C_{3v} and C_s symmetry

C_{2v}		C_{3v}		C_s	
Symmetry	Frequencies*	Symmetry	Frequencies	Symmetry	Frequencies
A_1	2170.1 (2183)	A_1	2160.1	A′	1990.0
A_1	2122.0 (2144)	A_1	2119.0	A′	1925.0
B_1	2120.6 (2137)	E	2104.8	A′	1916.5
B_2	2104.5 (2119)	–	–	A″	1916.4
ν(N-O)	1960.2 (1904)	ν(N-O)	1976.4	ν(N-O)	1586.7

*Values in brackets are experimental values taken from Ref. 36.

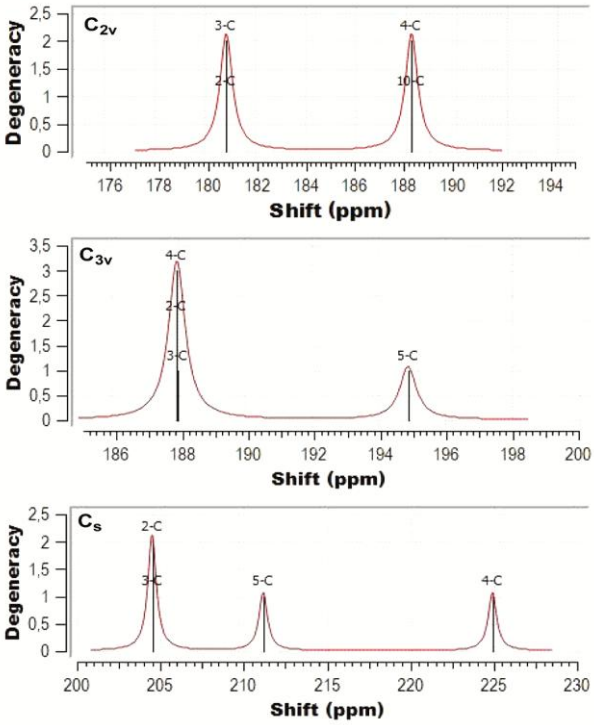

Fig. 4 — ^{13}C NMR spectra of the complexes with C_{2v}, C_{3v} and C_s symmetry calculated at the GIAO-BVP86/LANL2DZ/6-31G(d) level

2C-3C and 4C-10C replace each other and are considered as equivalent atoms.

In the ^{13}C NMR spectrum of the complex with C_{3v} symmetry, there are two peaks with different degeneracy. According to this spectrum, 2C, 3C and 4C carbon atoms are equivalent. As can be seen from Fig. 2, these carbon atoms are in the equatorial position. When the molecule with C_{3v} symmetry is rotated 120° around a C_3 axis passing through the Fe1-N10-O11 bond axis, these carbon atoms replace each other and are equivalent atoms. In the C_{3v} complex, there is no other carbon atom to which 5C is equivalent.

The carbon atoms in the Cs symmetry complex are in three different chemical environments. In this complex, there is only the identity operation and the plane of symmetry. As can be seen from Fig. 2, the symmetry plane passes through the 2C-Fe1-3C bond bisector. When the molecule is reflected from this plane, 2C and 3C replace each other. Atoms that replace each other only by reflecting from a plane of symmetry are called enantiotopic atoms. Since enantiotopic atoms also give NMR peak at the same chemical shift value, 2C and 3C have the same chemical shift value. As seen in Fig. 4, NMR peak

Table 4 — ^{13}C NMR chemical shift (δ) values and Mulliken charges of carbon atoms in complexes with C_{2v}, C_{3v} and C_s symmetry

Symmetry	Labeling	δ (ppm)	Mulliken charge
C_{2v}	2C=3C (eq)	180.9	+0.290
	4C=10C (ax)	188.2	+0.389
C_{3v}	2C=3C=4C (eq)	187.9	+0.283
	5C (ax)	194.9	+0.437
C_s	2C=3C (eq)	204.5	+0.226
	5C (eq)	211.2	+0.209
	4C (ax)	224.9	+0.228

intensities or degeneracy are directly proportional to the equivalent atomic numbers. According to these evaluations, it can be said that the geometry of the central atom in the complexes is triangular bipyramidal. The chemical shift values of the carbon atoms in the complexes and the Mulliken charges of the carbon atoms are given in Table 4.

As can be seen from Table 4, the chemical shift values of carbon atoms in the equatorial position in complexes with C_{2v}, C_{3v} and C_s point group are lower than those in the axial position. A low chemical shift value indicates that the atomic nucleus is highly shielded. One of the parameters showing the shielding of the atomic nucleus by electrons is the electronic charge of the atoms. When Table 4 is examined, it is seen that the electronic charges of the carbon atoms in the equatorial position are lower than the carbon atoms in the axial position. Equatorial carbons are then more shielded. The ^{13}C NMR chemical shift values of the carbon atoms in the equatorial position are low because the highly shielded nuclei peak at low ppm. In the literature, the experimentally measured ^{13}C NMR chemical shift for the complex with C_{2v} symmetry is given as 191.8 ppm, without axial-equatorial position distinction[36]. This value is quite compatible with the calculated 4C=10C chemical shift value.

Electronic properties of the complexes

The energy of the orbitals and the contour diagram can be considered to explain the electronic properties of the complexes. The ordering of the molecular orbitals according to their increasing energy is called the molecular orbital energy diagram. The functional orbitals in the molecular orbital energy diagram are usually the highest occupied molecular orbital (HOMO) and the lowest unoccupied molecular orbital (LUMO). These orbitals are known as frontier molecular orbitals. The molecular orbital energy diagrams of the complexes considered in this study

were calculated at the BVP86/LANL2DZ/6-31G(d) level and the energy diagrams for their orbitals between HOMO-2 and LUMO+2 are given in Fig. 5.

In Fig. 5, molecular orbital energies are in Hartree units. 1 Hartree unit is equal to 27.2116 electron Volts. As seen in Fig. 5, orbital 43 is HOMO and orbital 44 is LUMO for complexes with C_{2v} and C_{3v} point groups. For the complex with the C_s point group, orbital 44 is HOMO and orbital 45 is LUMO. These orbitals are frontier orbitals. According to Koopmans theorem, the energies of the HOMO and LUMO orbitals are related to the ionization energies (I) and electron affinities (A) of the complexes as given in Eq. (8)-(9)[50].

$$I = -E_{HOMO} \quad \text{... (8)}$$

$$A = -E_{LUMO} \quad \text{... (9)}$$

According to these equations, the ionization energy and electron affinity orders of the complexes are $I(C_s)<I(C_{3v})<I(C_{2v})$ and $A(C_s)<A(C_{2v})<A(C_{3v})$. The fact that both the ionization energy and electron affinity of the complex with Cs symmetry is the lowest may be related to its negative charge.

According to the linear combination of atomic orbitals method, a molecular orbital has the properties of the atomic orbitals that contribute most to it[49]. The contributions of atomic orbitals to a molecular orbital are determined from the wave function coefficients. Diagrams created by considering the wave function coefficients of an orbital are also called contour diagrams of orbitals. To explain the electronic properties of the complexes, contour diagrams of their frontier orbitals were obtained and together with their energies are given in Fig. 6.

As can be seen in Fig. 6, in general, central iron atom orbitals and π* molecular orbitals of CO/NO make the highest contribution to HOMO in complexes, while π* molecular orbitals of NO make the highest contribution to LUMO.

Some molecular properties of complexes

Molecular properties such as optical conductivity (ΔE), hardness (η), Mulliken electronegativity (χ), and electrophilicity index (ω) depend on the geometrical structures of the molecules. These properties of the complexes whose molecular structures were determined in this study were calculated from Equation (1)-(4) and their values are given in Table 5.

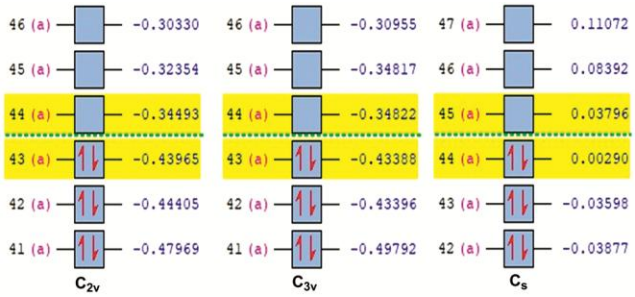

Fig. 5 — Energy diagrams of orbitals between HOMO-2 and LUMO+2 of complexes with C_{2v}, C_{3v} and C_s point groups

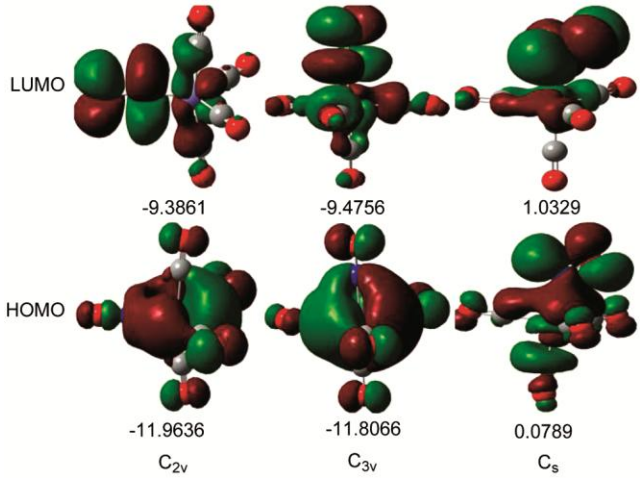

Fig. 6 — Contour diagrams of the frontier orbitals of complexes with C_{2v}, C_{3v} and C_s symmetry and their energies (eV)

Table 5 — Some molecular properties of the complexes with C_{2v}, C_{3v} and C_s point groups

	C_{2v}	C_{3v}	C_s
ΔE (eV)	2.5775	2.3310	0.9540
η (eV)	1.2887	1.1655	0.4770
χ (eV)	10.6748	10.6411	–0.5559
ω (eV)	44.2104	48.5770	0.3239

The energy difference between frontier molecular orbitals or energy gap (ΔE) has an important role in predicting the functions of molecules in reactions, their UV-VIS spectra, electrical and optical conductivity[51]. A decrease in the gap between the frontier orbitals means an increase in optical conductivity[52]. As can be seen in Table 5, the order of the complexes according to the increasing energy gap is $\Delta E(C_s)<\Delta E(C_{3v})<\Delta E(C_{2v})$. According to this order, it can be said that the optical conductivity of the complex with C_s symmetry is higher than the others. Considering that the energy gap of intrinsic semiconductor silicon is around 1.11 eV, it can be evaluated that the complex with C_s point group has

even higher intrinsic semi conductivity than silicon[53]. Since the conductivity of intrinsic semiconductors can be greatly increased by processes such as increasing the temperature, irradiation and doping, it can be said that the complex with C_s symmetry can have a significant optical conductivity.

The ordering of the complexes with C_{2v}, C_{3v} and C_s symmetry according to their hardness and Mulliken electronegativity is the same as the energy gap order. That is, the hardness and Mulliken electronegativity of the C_s complex are considerably lower than those of the complexes with C_{2v} and C_{3v} symmetry. Considering softness as the inverse of hardness, it is found that the softness of the complex with C_s symmetry is higher than that of the other complexes. Therefore, according to the hard-soft acid-base concept, it can be said that the C_s complex has a higher tendency to react with soft species[50]. When the calculated Mulliken electronegativities are examined, it is seen that the Mulliken electronegativity of the complex with C_s point group is considerably lower than that of the complexes with C_{2v} and C_{3v} symmetry.

The electrophilicity index is a quantitative measure of the tendency of a molecule to behave as an electrophile. The inverse of the electrophilicity index can be thought of as the nucleophilicity index. So, the electrophilicity index is inversely proportional to the nucleophilicity index. As seen in Table 5, the order of the electrophilicity index of the complexes is $\omega(C_s)<\omega(C_{2v})<\omega(C_{3v})$. In addition, the electrophilicity index of the complex with Cs symmetry is considerably lower than that of the others, indicating that the complex will act as a nucleophile.

Acidic and basic behavior of complexes can be predicted according to molecular orbital theory. According to the molecular orbital theory, the acidity of a molecule depends on the energy of HOMO and its basicity depends on the energy of LUMO. Species with higher HOMO energy than others behave basic, while species with lower LUMO energy than others behave acidic[49]. When the frontier orbital energies given in Fig. 5 are examined, the HOMO energy order is $C_{2v}<C_{3v}<C_s$, while the LUMO energy order is $C_{3v}<C_{2v}<C_s$. The HOMO energy of the C_s complex is considerably higher than that of the other complexes. Therefore, the complex with Cs symmetry behaves more basic than the others.

Conclusions

eq-$[Fe(CO)_4(NO)]^+$ (C_{2v}), ax-$[Fe(CO)_4(NO)]^+$ (C_{3v}), eq-$[Fe(CO)_4(NO)]^-$ (C_s) and ax-$[Fe(CO)_4(NO)]^-$ (C_s) complexes were designed. The optimal computational level was determined as BVP86/LANL2DZ/6-31G(d) using the experimental C-O stretching frequencies of the complex with C_{2v}point group. It was found that the eq-$[Fe(CO)_4(NO)]^-$ (C_s) complex was converted to the ax-$[Fe(CO)_4(NO)]^-$ (C_s) complex during the optimization process. From the molecular structure parameters, IR and ^{13}C NMR spectra, it was determined that the central iron atom in the complexes was in the triangular bipyramidal ligand field. It was estimated from the Fe-C, C-O bond lengths and C-O bond stretching frequencies that the CO-releasing material properties of the complexes with C_{2v} and C_{3v} symmetry were higher than those of the complex with C_s symmetry. From the calculated molecular descriptors, the optical conductivity, softness, nucleophilicity and basicity strength of the C_s complex were found to be higher than those of the other complexes.

Acknowledgments

The authors are grateful for their support to the Sivas Cumhuriyet University, Scientific Research Unit (Project No: F-2022-663).

References

1 Delville-Desbois M-H, Mross S, Astruc D, Linares J, Varret F, Le Beuze A, Saillard J-Y, Culp R D, Atwood D A & Cowley A H, *J Am Chem Soc*, 118 (17) (1996) 4133.
2 Hsu H F, Koch S A, Popescu C V & Münck E, *J Am Chem Soc*, 119 (35) (1997) 8371.
3 Nakae T, Hirotsu M, Aono S & Nakajima H, *J Chem Soc, Dalton Transactions*, 45 (41) (2016) 16153.
4 Nakae T, Hirotsu M & Nakajima H, *Inorg Chem*, 57 (14) (2018) 8615.
5 Javaheri S & Glering W P, *Organometallics*, 3 (12) (1984) 1927.
6 Jiang X, Xiao Z, Zhong W & Liu X, *Coord Chem Rev*, 429 (2021) 213634.
7 Petricci E, Santillo N, Castagnolo D, Cini E & Taddei M, *Advanced Synthesis & Catalysis*, 360 (13) (2018) 2560.
8 Loewen N D, Neelakantan T V & Berben L A, *Accts Chem Res*, 50 (9) (2017) 2362.
9 Bromfield K M, Gradén H, Ljungdahl N & Kann N, *J Chem Soc Dalton Transactions*, 5051 (2009).
10 Kochetkov K A, Vasil T T, Gasanov R G, Mysova N E & Bystrova N A, *Russian Chem Bull*, 68 (7) (2019) 1301.
11 Beesu M & Periasamy M, *J Organomet Chem*, 705 (2012) 30.
12 Wombwell C, Caputo C A & Reisner E, *Accts Chem Res*, 48 (11) (2015) 2858.
13 Peters J W, Lanzilotta W N, Lemon B J & Seefeldt L C, *Science*, 282 (5395) (1998) 1853.
14 Nicolet Y, Piras C, Legrand P, Hatchikian C E & Fontecilla-Camps J C, *Structure*, 7 (1) (1999) 13.

15 Shima S, Pilak O, Vogt S, Schick M, Stagni M S, Meyer-Klaucke W, Warkentin E, Thauer R K & Ermler U, *Science*, 321 (5888) (2008) 572.
16 Basu U, Roy M & Chakravarty A R, *Coord Chem Rev*, 417 (2020) 213339.
17 Gonzales M A & Mascharak P K, *J Inorg Biochem*, 133 (2014) 127.
18 Pinto M N & Mascharak P K, *J Photochem Photobiol C*: *Photochemistry Reviews*, 42 (2020) 100341.
19 Adach W, Błaszczyk M & Olas B, *Chemico-Biological Interactions*, 318 (2020) 108973.
20 Kourti M, Jiang W G & Cai J, *Oxidative Medicine and Cellular Longevity*, 2017 (2017).
21 Wareham L K, Begg R, Jesse H E, Van Beilen J W A, Ali S, Svistunenko D, McLean S & Poole R K, *Antioxidants and Redox Signaling*, 24 (17) (2016) 1013.
22 Kohmoto J, Nakao A, Kaizu T, Tsung A, Ikeda A, Tomiyama K, Billiar T R, Choi A M K, Murase N & McCurry K R, *Surgery*, 140 (2) (2006) 179.
23 Volti G L, Rodella L F, Di Giacomo C, Rezzani R, Bianchi R, Borsani E & Motterlini R, *Nephron Experimental Nephrology*, 104 (4) (2006) e135-e139.
24 Motterlini R, Gonzales A, Foresti R, Clark J E, Green C J & Winslow R M, *Circ Res*, 83 (1998) 568.
25 Omaye S T, *Toxicology*, 180 (2) (2002) 139.
26 Appleton S D, Chretien M L, McLaughlin B E, Vreman H J, Stevenson D K, Brien J F & Marks G S, *Drug Metabolism and Disposition*, 27 (10) (1999) 1214.
27 Mann B E, 'Carbon monoxide: An essential signalling molecule' in, *Medicinal Organometallic Chemistry* (Springer, Berlin, Heidelberg), pp.247-285 (2010).
28 Kuypers M M, Marchant H K & Kartal B, *Nature Reviews Microbiology*, 16 (5) (2018) 263.
29 Keilwerth M, Hohenberger J, Heinemann F W, Sutter J, Scheurer A, Fang H, Bill E, Neese F, Ye S & Meyer K, *J Am Chem Soc*, 141 (43) (2019) 17217.
30 Pacher P, Beckman J S & Liaudet L, *Physiological Rev*, 87 (1) (2007) 315.
31 Hoffman B M, Lukoyanov D, Yang Z Y, Dean D R & Seefeldt L C, *Chem Rev*, 114 (8) (2014) 4041.
32 Fitzpatrick J & Kim E, *Accts Chem Res*, 48 (8) (2015) 2453.
33 Berto T C, Speelman A L, Zheng S & Lehnert N, *Coord Chem Rev*, 257 (1) (2013) 244.
34 In-Iam A, Wolf M, Wilfer C, Schaniel D, Woike T & Klüfers P, *Chemistry-A European Journal*, 25 (5) (2019) 1304.
35 Enemark J H & Feltham R D, *Coord Chem Rev*, 13 (4) (1974) 339.
36 Bohnenberger J & Krossing I, *Angew Chem Int Ed*, 59 (14) (2020) 5581.
37 Zadrozny J M, Xiao D J, Atanasov M, Long G J, Grandjean F, Neese F & Long J R, *Nature Chemistry*, 5 (7) (2013) 577.
38 Samuel P P, Mondal K C, Sheik N A, Roesky H W, Carl E, Neufeld R, Stalke D, Demeshko S, Meyer F, Ungur L, Chibotaru L F, Christian J, Ramachandran V, van Tol J & Dalal N S, *J Am Chem Soc*, 136 (34) (2014) 11964.
39 Dennington R D, Keith T A & Millam J M, GaussView 6.0. 16, Semichem. Inc., Shawnee Mission KS, 2016.
40 Frisch M J, Trucks G W, Schlegel H B, Scuseria G E, Robb M A, Cheeseman J R & Nakatsuji H, Gaussian09 Revision D. 01, Gaussian Inc., Wallingford CT, 2009, See also: URL: http://www.gaussian.com
41 Becke A D, *Physical Review A*, 38 (6) (1988) 3098.
42 Perdew J P, *Physical Review B*, 34 (10) (1986) 7406.
43 Yang Y, Weaver M N & Merz K M Jr, *J Phys Chem A*, 113 (36) (2009) 9843.
44 Csonka G I, *J Mol Str*: *THEOCHEM*, 584 (1-3) (2002) 1.
45 Erkan S & Karakaş D, *J Mol Str*, 1199 (2020) 127054.
46 Huheey J E, *Inorg Chem*, 20 (11) (1981) 4033.
47 Karakaş D & Kaya C, *J Organomet Chem*, 640 (1-2) (2001) 37.
48 Kaya C & Karakas D, *Indian J Chem*, 46A (1) (2007) 33.
49 Orchin M & Jaffé H H, *Symmetry*, *Orbitals and Spectra* (*SOS*) (Wiley-Interscience) (1971).
50 Pearson R G, *Inorg Chem*, 27 (4) (1988) 734.
51 Fleming I, *Frontier Orbitals and Organic Chemical Reactions* (John Wiley and Sons, London, UK) (1977).
52 Woods-Robinson R, Han Y, Zhang H, Ablekim T, Khan I, Persson K A & Zakutayev A, *Chem Rev*, 120 (9) (2020) 4007.
53 Haynes W M, *CRC Handbook of Chemistry and Physics*, Vol. 9, edited by D R Lide (CRC Press, Boca Raton, FL) (2010).